ELSEVIER

Journal of Quantitative Spectroscopy & Radiative Transfer 106 (2007) 262–273

Journal of Quantitative Spectroscopy & Radiative Transfer

www.elsevier.com/locate/jqsrt

Scattering and radiative properties of complex soot and soot-containing aggregate particles

Li Liu[a,b], Michael I. Mishchenko[a,*]

[a]*NASA Goddard Institute for Space Studies, 2880 Broadway, New York, NY 10025, USA*
[b]*Department of Applied Physics and Applied Mathematics, Columbia University, New York, NY 10025, USA*

Abstract

We use the superposition *T*-matrix method to compute the scattering matrix elements and optical cross-sections for a variety of complex soot and soot-containing aggregate particles in random orientation at a visible wavelength 0.628 μm. It is shown that random variations in the geometrical configuration of monomers in a soot cluster for fixed fractal dimension and prefactor, monomer size, and number of monomers have a rather weak effect on scattering and absorption, at least in the visible part of the spectrum. Thus, the electromagnetic scattering and absorption characteristics of a single cluster realization are sufficient to represent the mean values obtained by averaging over many realizations of the "equivalent" clusters generated for the same fractal parameters. However, the results for the soot clusters differ fundamentally from those calculated for the volume-equivalent soot sphere and for the corresponding external mixture of soot monomers, assuming that there are no electromagnetic interactions between the monomers. We also compute and analyze the scattering and absorption properties of aerosols formed by semi-external aggregation of larger ammonium sulfate, silica, or dust particles with soot clusters as well as semi-external aggregates consisting of several components with different sizes and refractive indices. Depending on its chemical composition and size, the larger particle that is in touch with a soot cluster can strongly influence, or even dominate, the overall optical characteristics of the aggregate. Aggregation can result in stronger extinction, absorption, and scattering cross-sections relative to those computed for the corresponding external mixture. Possibly owing to mutual shadowing, the optical cross-sections of multi-component aggregates are smaller than those of their externally mixed counterparts, but by no more than ~20%. Implications of our study for analyses of remote sensing observations and atmospheric radiation balance computations are discussed.
Published by Elsevier Ltd.

Keywords: Aggregates; Scattering; Optical cross-sections; Single-scattering albedo; Asymmetry parameter; Scattering matrix; Polarization; Remote sensing; Atmospheric radiation

1. Introduction

Tropospheric aerosols often exhibit nonspherical overall shapes and complex morphologies (e.g., [1–7]), which poses a tremendous challenge in particle characterization and global climate modeling studies. The effects of particle nonsphericity on electromagnetic scattering, remote-sensing retrievals, and atmospheric

*Corresponding author. Tel.: +1 212 678 5590; fax: +1 212 678 5622.
E-mail address: crmim@giss.nasa.gov (M.I. Mishchenko).

0022-4073/$ - see front matter Published by Elsevier Ltd.
doi:10.1016/j.jqsrt.2007.01.020

radiation balance computations have been extensively studied in the literature (e.g., [8–14] and references therein). Recently, we have used the superposition T-matrix method [15,16] to analyze potential effects of aggregation and heterogeneity on light scattering and absorption by morphologically complex tropospheric aerosols [17,18]. Those studies were motivated by the well-known fact that different kinds of tropospheric aerosols (e.g., dust, carbonaceous, and sulfate particles) can be suspended in air not only in the form of external mixtures (different aerosol particles are separated by distances much greater than their sizes and scatter light independently of each other) but also in the form of semi-external mixtures (two or more aerosol particles are in physical contact and form an aggregate) and even internal mixtures (one or several small aerosol particles are imbedded in a larger host particle).

It is well known that dry soot particles tend to exist in the form of clusters potentially consisting of hundreds of tiny monomers, as illustrated in Fig. 1(a). It was demonstrated by Liu and Mishchenko [18] that the effects of aggregation, fractal morphology, and refractive index on the integral extinction, scattering, and absorption properties of soot aerosols can be quite significant. The nearly isotropic Rayleigh phase function typical of the individual spherules also undergoes a drastic change and evolves into a (strongly) forward-scattering phase function representative of wavelength-sized scatterers. Those results suggest that the cluster structure of soot aerosols must be explicitly taken into account in remote sensing and radiation balance applications.

Despite the unequivocal relevance and significance of the conclusions drawn in [18], that study remains somewhat limited in that it did not address a factor potentially affecting the optical properties of a polydispersion of soot clusters. Specifically, we used the traditional approach of defining the morphology of a cluster by the number of monomers, their size, the prefactor, and the fractal dimension [19] and based our conclusions on computations of electromagnetic scattering and absorption for only one realization of a cluster rendered by the fractal-particle generator for given fractal parameters. However, the specification of the fractal parameters does not yield a unique cluster shape (see Fig. 1). This obviously necessitates an extension of [18] wherein the results are averaged over several cluster realizations obtained for the same fractal parameters (cf. [20]). Another straightforward extension of [18] is to quantify and analyze the errors caused by employing the simple volume-equivalent-sphere model as well as the external mixing approximation frequently used to represent the scattering and absorption properties of a soot cluster.

It has also been demonstrated that dry soot clusters may tend to aggregate with relatively large ammonium sulfate or silica particles, as shown in Fig. 2(a). Even more complex semi-external aggregates consisting of

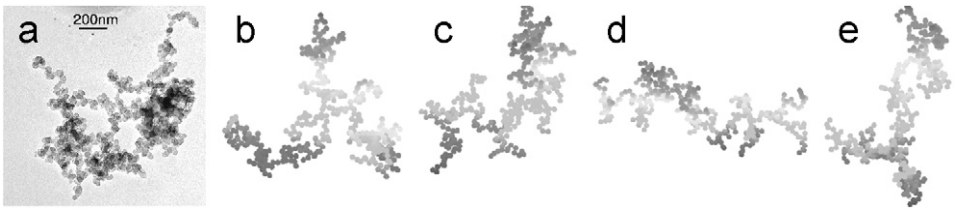

Fig. 1. (a) TEM image of a soot cluster [2]. (b)–(e) Soot clusters with $N_s = 400$, $k_0 = 1.19$, and $D_f = 1.82$, as generated by the algorithm developed by Mackowski [13].

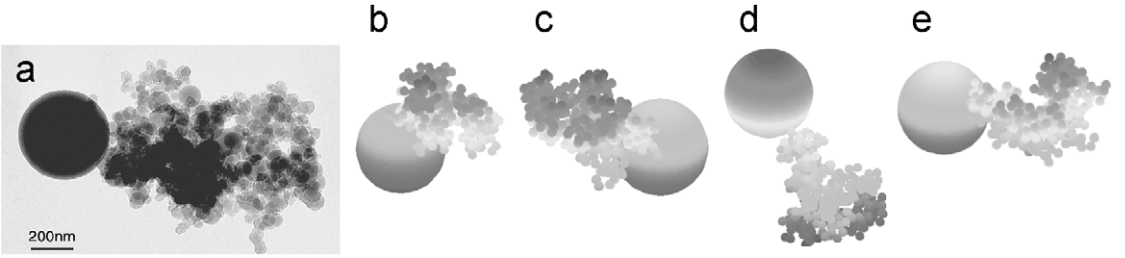

Fig. 2. (a) TEM image of an aggregate formed by a soot cluster and an ammonium sulfate particle [2]. (b)–(e) Aggregates formed by fractal soot clusters ($D_f = 2.4$, $k_0 = 1.19$, $N_s = 300$, $a = 0.02\,\mu m$, and $m = 1.75 + i0.435$) attached to a larger aerosol particle.

more than two chemical components have often been encountered in various field campaigns (e.g., [2,7]). Therefore, another objective of this paper is to compute and analyze the scattering and absorption properties of these specific types of complex aerosols.

2. Methodology

The superposition T-matrix code used in our computations was documented in [15] and is publicly available at http://www.giss.nasa.gov/~crmim/t_matrix.html. The critical advantages of this as well as the other T-matrix codes available at the above web site are that they are numerically exact, much more efficient than any other numerical techniques based on an explicit solution of the Maxwell equations, can be applied to a wide range of particle sizes, shapes, and morphologies, and generate all scattering and absorption characteristics of particles necessary to interpret the results of any in situ and remote sensing observations as well as to compute the radiative energy balance [21].

The key single-scattering characteristics of randomly oriented particles forming a macroscopically isotropic and mirror-symmetric medium are the ensemble-averaged scattering, $C_{\rm sca}$, and extinction, $C_{\rm ext}$, cross-sections and the elements of the normalized scattering matrix [16]. In the standard $\{I, Q, U, V\}$ representation of polarization, the normalized Stokes scattering matrix has the well-known block-diagonal structure [16,22]:

$$\tilde{\mathbf{F}}(\Theta)=\begin{bmatrix} a_1(\Theta) & b_1(\Theta) & 0 & 0 \\ b_1(\Theta) & a_2(\Theta) & 0 & 0 \\ 0 & 0 & a_3(\Theta) & b_2(\Theta) \\ 0 & 0 & -b_2(\Theta) & a_4(\Theta) \end{bmatrix}, \tag{1}$$

where $0^\circ \leqslant \Theta \leqslant 180^\circ$ is the scattering angle. The (1, 1) element of the scattering matrix, $a_1(\Theta)$, is traditionally called the phase function and satisfies the following normalization condition:

$$\frac{1}{2}\int_0^\pi \mathrm{d}\Theta \sin\Theta a_1(\Theta)=1. \tag{2}$$

Another useful quantities are the ensemble-averaged absorption cross-section, $C_{\rm abs}=C_{\rm ext}-C_{\rm sca}$, the single-scattering albedo, $\varpi=C_{\rm sca}/C_{\rm ext}$, and the asymmetry parameter defined by

$$\langle\cos\Theta\rangle=\frac{1}{2}\int_0^\pi d\Theta\ \sin\Theta a_1(\Theta)\cos\Theta. \tag{3}$$

In this study, all computations of light scattering and absorption by complex soot or soot containing aggregates have been performed at a fixed visible wavelength 0.628 μm.

3. Ensemble averaging for fractal-parameter-equivalent soot clusters

The parameters used to describe the morphology of a soot cluster include the fractal prefactor k_0, the fractal dimension $D_{\rm f}$, the number of monomers in the cluster $N_{\rm S}$, and the monomer mean radius a. They are related by the following statistical scaling law [19,23]:

$$N_{\rm S}=k_0\left(\frac{R_{\rm g}}{a}\right)^{D_{\rm f}}, \tag{4}$$

where $R_{\rm g}$, called the radius of gyration, is a measure of the overall aggregate radius. On the log–log plot of $N_{\rm S}$ versus $R_{\rm g}/a$ for a set of aggregates, the fractal dimension and the prefactor describe the slope and the intercept of the least-square linear regression fit, respectively. We have used the random fractal cluster generator described in [13] to create 20 fractal-parameter-equivalent soot clusters composed of 400 equal-size monomers for the same values of the prefactor ($k_0=1.19$) and fractal dimension ($D_{\rm f}=1.82$). These fixed $D_{\rm f}$ and k_0 values are the means obtained by Sorensen and Roberts [24] in their diffusion-limited cluster aggregation simulations. Four of these clusters are shown in Fig. 1 and reveal significant morphological differences. The radius of the soot monomers a is fixed at 0.02 μm, which is a typical spherule size observed in experiments (e.g.,

[3,25]). Consistent with our previous study [18], the following two values of the refractive index m are used to represent the various types of soot: $1.75+i0.435$ [26] and $2+i$ (soot G adopted by Fuller et al. [12]).

The ensemble-averaged values are obtained using the following formulas:

$$C_{\rm ext} = \frac{1}{N}\sum_{i=1}^{N} C_{\rm ext}^{i}, \tag{5}$$

$$C_{\rm sca} = \frac{1}{N}\sum_{i=1}^{N} C_{\rm sca}^{i}, \tag{6}$$

$$g = \frac{\sum_{i=1}^{N} g^{i} C_{\rm sca}^{i}}{N C_{\rm sca}}, \tag{7}$$

where $C_{\rm ext}$, $C_{\rm sca,}$ and g are the average extinction and scattering cross-sections and asymmetry parameter, respectively, $C_{\rm ext}^{i}$, $C_{\rm sca}^{i}$, and g^{i} are the extinction and scattering cross-sections and asymmetry parameter, respectively, for the ith fractal realization, and $N=20$. The elements of the ensemble-averaged normalized Stokes scattering matrix are obtained by

$$a_p(\Theta) = \frac{1}{N C_{\rm sca}}\sum_{i=1}^{N} a_p^{i}(\Theta)\, C_{\rm sca}^{i}, \quad p = 1,\ 2,\ 3,\ 4, \tag{8}$$

$$b_p(\Theta) = \frac{1}{N C_{\rm sca}}\sum_{i=1}^{N} b_p^{i}(\Theta) C_{\rm sca}^{i}, \quad p = 1, 2, \tag{9}$$

where, again, $a_1^{i}(\Theta), a_2^{i}(\Theta), a_3^{i}(\Theta), a_4^{i}(\Theta), b_1^{i}(\Theta)$, and $b_2^{i}(\Theta)$ are the scattering-matrix elements for the ith fractal realization. The average quantities are then compared with those obtained with the frequently used external mixing scheme (assuming that all spherules are widely separated) and the simple model wherein a homogeneous volume-equivalent sphere is used to represent the scattering and absorption properties of a soot cluster.

Table 1 demonstrates that the differences in the integral photometric characteristics (the extinction, scattering, and absorption cross-sections, the single-scattering albedo, and the asymmetry parameter) among the different fractal-parameter-equivalent soot clusters are rather small. Indeed, the standard deviation relative to the corresponding mean does not exceed 3.5%, with particularly small differences in the extinction and absorption cross-sections. However, the ensemble-averaged characteristics differ fundamentally from those calculated for the "equivalent" external mixtures. Clustering results in a rather significant enhancement of extinction and absorption relative to the case of independently scattering spherules. Yet the most profound effect of aggregation is on the single-scattering albedo and the asymmetry parameter as well as on the scattering cross-section (cf. [18]). The optical properties of the clusters are also significantly different from those of the volume-equivalent homogeneous spheres. Overall, the clusters have a larger asymmetry parameter, but smaller extinction and scattering cross-sections and single-scattering albedo than those of the volume-equivalent spheres. The cluster absorption cross-section can be either smaller or greater than that of the equal-volume sphere, depending on the choice of the soot refractive index.

Fig. 3 illustrates the morphology-caused variability in the scattering matrix elements for the 20 fractal-parameter-equivalent clusters. The relative differences (standard deviation versus mean) in the phase function $a_1(\Theta)$ and in the $a_2(\Theta)$ and $b_1(\Theta)$ elements are less than 15%. The variations in $a_3(\Theta)$ and $a_4(\Theta)$ are also small. Overall, the standard deviations versus the mean values for these two elements do not exceed 15% except at scattering angles between 89° and 94°, where the $a_3(\Theta)$ and $a_4(\Theta)$ values are very close to 0. The relative differences in $b_2(\Theta)$ are rather significant, partly due to the small magnitude of this scattering matrix element. Thus, even though the $b_2(\Theta)$ element appears to be fractal-morphology sensitive, its experimental detection is obviously problematic [27].

We can, therefore, conclude that the electromagnetic scattering and absorption properties calculated for only one realization of a soot cluster for given $D_{\rm f}$, k_0, and $N_{\rm S}$ values can be used to represent the optical

Table 1
Integral photometric characteristics of fractal-parameter-equivalent soot clusters for two values of the soot refractive index

$m = 1.75 + i0.435$	Ensemble-averaged value		C_{ext} (μm^2)	C_{abs} (μm^2)	C_{sca} (μm^2)	g	ϖ
			0.0980	0.0815	0.0165	0.6661	0.1685
	Ratio		Extinction	Absorption	Scattering	AP[a]	SSA[b]
		Std/mean (%)[c]	0.5483	0.1463	3.4213	2.3858	2.8711
		Ext/cluster[d]	0.7475	0.8930	0.0293	0.0130	0.0392
		VES/cluster[e]	1.7100	1.1618	4.4159	0.7795	2.5824
$m = 2 + i$	Ensemble-averaged value		C_{ext} (μm^2)	C_{abs} (μm^2)	C_{sca} (μm^2)	g	ϖ
			0.1857	0.1494	0.0362	0.6685	0.1951
	Ratio		Extinction	Absorption	Scattering	AP	SSA
		Std/mean (%)	0.4730	0.2925	3.0764	2.3844	2.6312
		Ext/cluster	0.6721	0.8279	0.0295	0.0130	0.0439
		VES/cluster	1.0798	0.7452	2.4600	0.6738	2.2783

[a]Asymmetry parameter.
[b]Single-scattering albedo.
[c]The ratio of one standard deviation to the corresponding value averaged over 20 "equivalent" cluster realizations.
[d]The ratios of the optical properties calculated for the external mixture to the corresponding cluster ensemble-averaged values.
[e]The ratios of the optical properties calculated for the volume-equivalent sphere to the corresponding cluster ensemble-averaged values.

properties of the entire ensemble of soot clusters having the same fractal parameters. This result is very important in practice since it can greatly reduce the computational effort; it will be further discussed in the following sections.

Fig. 4 compares the scattering matrix elements averaged over the 20 soot-cluster realizations with those computed for the corresponding external mixture and the homogeneous equal-volume sphere. Overall, the angular scattering properties of the soot clusters appear to be a peculiar mix of those of wavelength-sized particles (the nearly isotropic Rayleigh phase function for individual spherules evolves into a forward scattering phase function) and Rayleigh scatterers (i.e., the degree of linear polarization of scattered light for unpolarized incident light, $-b_1(\Theta)/a_1(\Theta)$, is zero at the exact forward-scattering and back-scattering directions and reaches a nearly 100% maximum at $\Theta \approx 90^\circ$ (cf. [28]), and the $b_2(\Theta)/a_1(\Theta)$ values are very close to zero). The deviation of the ratio $a_2(\Theta)/a_1(\Theta)$ from unity is a manifestation of the overall nonsphericity of the soot clusters [16]. Clearly, the independent-spherule model provides a poor representation of the cluster phase function, whereas the performance of the equal-volume-sphere model is inadequate with respect to all scattering matrix elements.

The angular patterns of the scattering matrix elements computed for the same clusters but with a more absorptive soot refractive index $2 + i$ are rather similar to those shown in Figs. 3 and 4 and will not be discussed here specifically.

4. Aggregates composed of soot clusters attached to a sulfate, silica, or dust particle

As demonstrated in the literature (e.g., [2] and references therein), soot clusters may tend to aggregate with ammonium sulfate, silica, dust or other aerosol particles. In the following, we will describe and analyze the scattering and absorption properties of such complex aerosols. Once again, the cluster-generation code developed by Mackowski [13] was used to simulate a soot cluster. We have fixed the fractal pre-factor at 1.19 and the fractal dimension at 2.4, thereby assuming rather compact clusters similar to that shown in Fig. 2(a). The number of monomers in each soot cluster was fixed at 300. After a soot cluster has been generated, it was randomly attached to a larger aerosol particle, thereby resulting in a specific realization of a chemically heterogeneous aggregate. We have generated a total of 20 such realizations for each type of larger particle. Four typical aggregates are shown in Figs. 2(b)–(e). The one shown in Fig. 2(e) appears to resemble the most the TEM image taken by Li et al. [2] over the North Atlantic, Fig. 2(a).

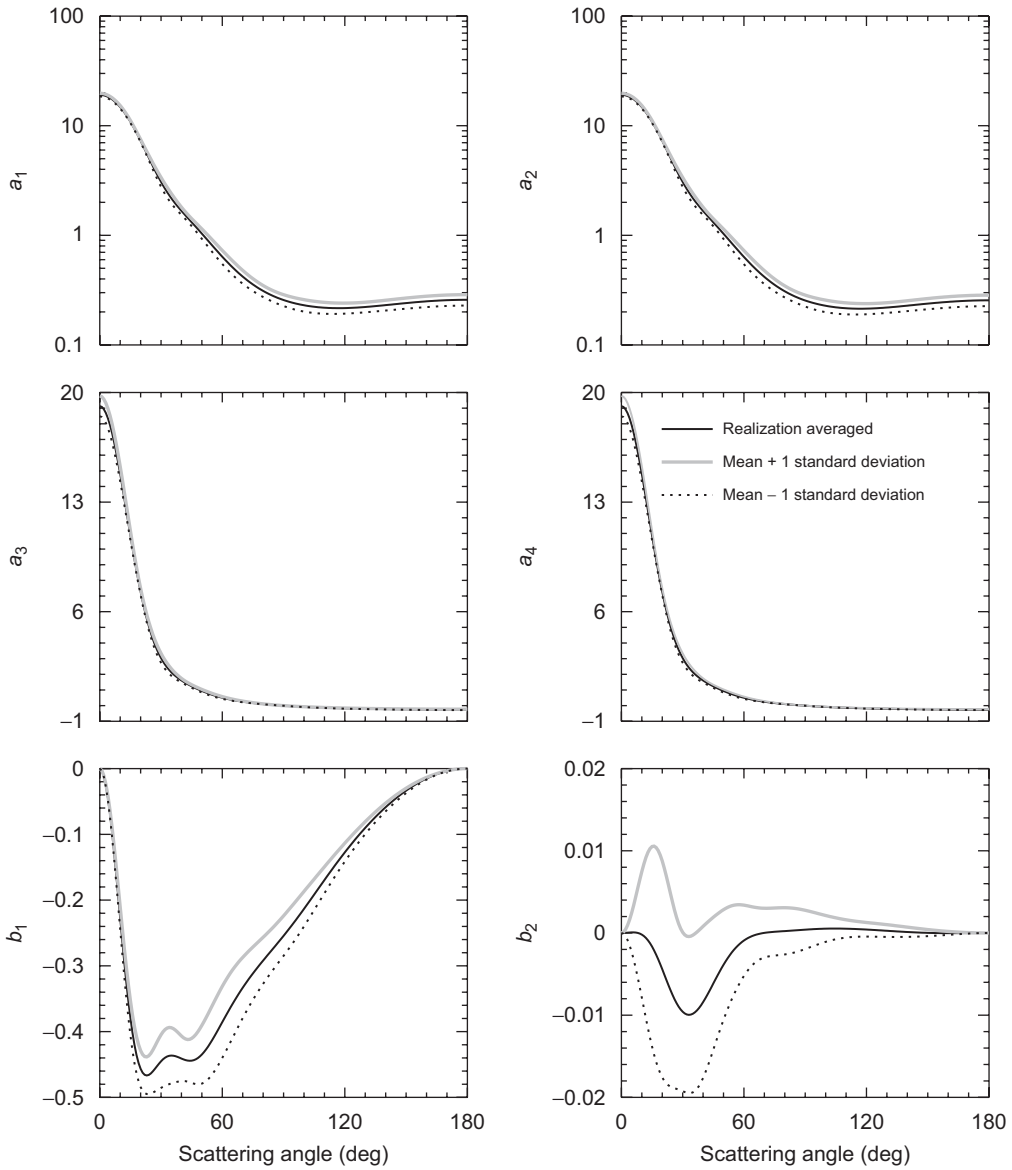

Fig. 3. Variability of the scattering matrix elements computed for 20 fractal-parameter-equivalent soot clusters with the refractive index $1.75+i0.435$. The fixed fractal parameters are as follows: $D_f = 1.82$, $k_0 = 1.19$, $N_S = 400$, and $a = 0.02\,\mu m$. Black, gray, and dotted curves depict the ensemble-averaged values, the averaged values plus one standard deviation, and the averaged values minus one standard deviation.

Table 2 summarizes the ensemble-averaged integral photometric characteristics of the complex aerosols formed by aggregation of soot clusters with a larger particle. The soot monomer radius is $0.02\,\mu m$, and the soot refractive index is fixed at $1.75+i0.435$. The larger particle is $0.2\,\mu m$ in radius and can be either an ammonium sulfate, silica, or dust particle with the respective refractive index 1.44 [26], 1.53 [29], or $1.53+i0.008$ [26].

It is seen that aggregation results in greater extinction, absorption, and scattering cross-sections compared with those computed for the corresponding external mixtures, but by no more than 19%. Changing the refractive index of soot from $1.75+i0.435$ to $2+i$ is expected to increase significantly the enhancement in the optical cross-sections. The differences in the single-scattering albedo and the asymmetry parameter are smaller. Obviously, the chemical composition and size of the larger particle have a pronounced effect on the

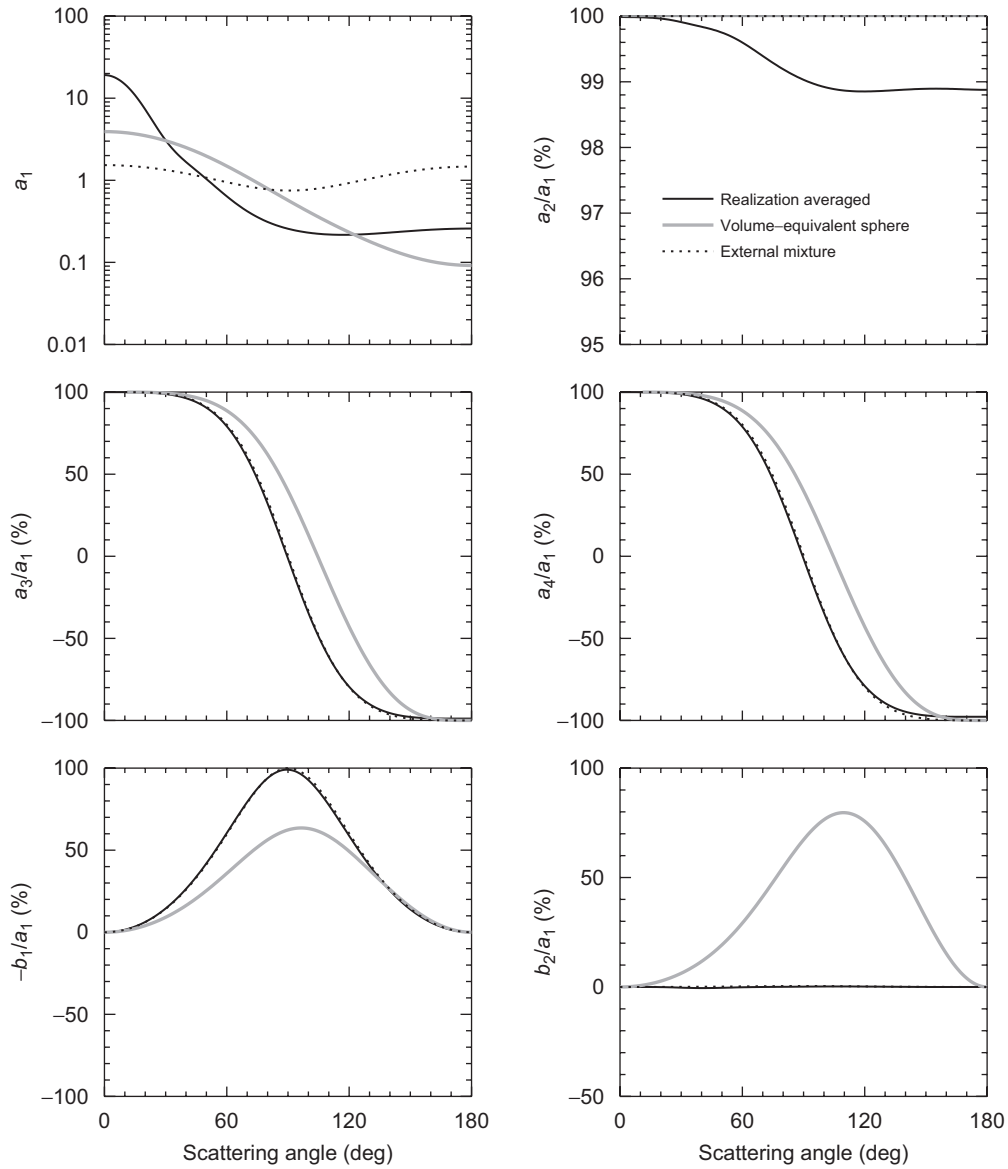

Fig. 4. Ensemble-averaged scattering matrix elements (black curves) versus scattering angle for fractals with $D_f = 1.82$, $k_0 = 1.19$, $N_S = 400$, and $a = 0.02\,\mu m$. The soot refractive index is $1.75 + i0.435$. The gray and dotted curves depict the Stokes scattering matrix elements computed for the corresponding homogeneous volume-equivalent sphere and the "equivalent" external mixture, respectively.

overall radiative properties of the aggregates. The one-standard-deviation spreads in the integral photometric characteristics among the 20 aggregate realizations are all smaller than 0.5%, which suggests again that a specific morphological configuration of an aggregate has negligible effect on the integral photometric characteristics.

Fig. 5 depicts the scattering matrix elements averaged over the 20 realizations of a soot–sulfate aggregate along with those computed for the corresponding external mixture as well as for the sulfate particle alone. The angular scattering characteristics calculated for the soot–silica and soot–dust aggregates are rather similar and will not be discussed specifically. It is quite obvious that the larger sulfate particle contributes considerably to the total scattering matrix of the aggregates. The total phase function is strongly forward-directed, which is typical of wavelength-sized scatterers. The degree of linear polarization $-b_1(\Theta)/a_1(\Theta)$ exhibits a rather broad

Table 2
Integral photometric characteristics calculated for ensembles of "equivalent" aggregates formed by soot clusters attached to an ammonium sulfate, silica, or dust particle[a]

Ammonium sulfate[b]	Ensemble-averaged value		C_{ext} (μm^2)	C_{abs} (μm^2)	C_{sca} (μm^2)	g	ϖ
			0.2658	0.0616	0.2042	0.6873	0.7683
	Ratio		Extinction	Absorption	Scattering	AP[c]	SSA[d]
		Std/mean (%)[e]	0.2672	0.2324	0.3255	0.4296	0.0824
		Ext/aggregate[f]	0.8533	0.8869	0.8431	0.9406	0.9881
Silica[g]	Ensemble-averaged value		C_{ext} (μm^2)	C_{abs} (μm^2)	C_{sca} (μm^2)	g	ϖ
			0.3464	0.0616	0.2848	0.6521	0.8221
	Ratio		Extinction	Absorption	Scattering	AP	SSA
		Std/mean (%)	0.2063	0.2598	0.2249	0.4098	0.0489
		Ext/aggregate	0.8900	0.8857	0.8909	0.9395	1.0010
Dust[h]	Ensemble-averaged value		C_{ext} (μm^2)	C_{abs} (μm^2)	C_{sca} (μm^2)	g	ϖ
			0.3466	0.0704	0.2763	0.6560	0.7970
	Ratio		Extinction	Absorption	Scattering	AP	SSA
		Std/mean (%)	0.2022	0.2324	0.2348	0.4143	0.0598
		Ext/aggregate	0.8910	0.9052	0.8873	0.9398	0.9959

[a]The soot refractive index is fixed at $1.75+i0.435$.
[b]The soot clusters are aggregated with a sulfate particle.
[c]Asymmetry parameter.
[d]Single-scattering albedo.
[e]The ratio of one standard deviation to the corresponding value averaged over 20 "equivalent" aggregate realizations.
[f]The ratios of the optical properties computed for the external mixture to the corresponding aggregate ensemble-averaged values.
[g]The soot clusters are aggregated with a silica particle.
[h]The soot clusters are aggregated with a dust particle.

negative region at scattering angles between 103° and 180°, whereas the nearly 100% polarization value at $\Theta \approx 90^\circ$ typical of individual soot clusters significantly weakens and shifts towards smaller scattering angles. Similarly, the $b_2(\Theta)/a_1(\Theta)$ ratio for the aggregates does not vanish, as it would nearly do in the case of individual soot clusters.

The scattering matrix elements computed for the corresponding external mixture and the individual sulfate particle are almost indistinguishable. This obviously happens because the larger sulfate particle dominates the cumulative scattering matrix. The significant scattering-matrix differences between the aggregates and the "equivalent" external mixture illustrate yet another failure of the conventional Lorenz–Mie theory to represent the scattering properties of morphologically complex aerosols.

5. Multi-component aggregates

In this section, we consider aggregates composed of two dust particles (refractive index $m = 1.53+i0.008$ and radii $r = 1.0$ and $0.6\,\mu m$), two equal-sized soot particles ($m = 1.75+i0.435$ and $r = 0.15\,\mu m$), and one sulfate particle ($m = 1.44$ and $r = 0.3\,\mu m$), as shown in Fig. 6. Once again, we have created 20 aggregate realizations to examine the potential effect of morphology on electromagnetic scattering by multi-component aggregates consisting of several semi-externally mixed aerosols.

Consistent with our previous study of two-component aggregates [17], Table 3 demonstrates that the differences in the integral photometric characteristics between the multi-component clusters and the composition-equivalent external mixture do not exceed 15% and are often much smaller, particularly for ϖ and g. Possibly owing to mutual shadowing [30], the scattering and absorption cross-sections of the aggregates are smaller than those of the external mixture. It is confirmed once again that changes in specific particle

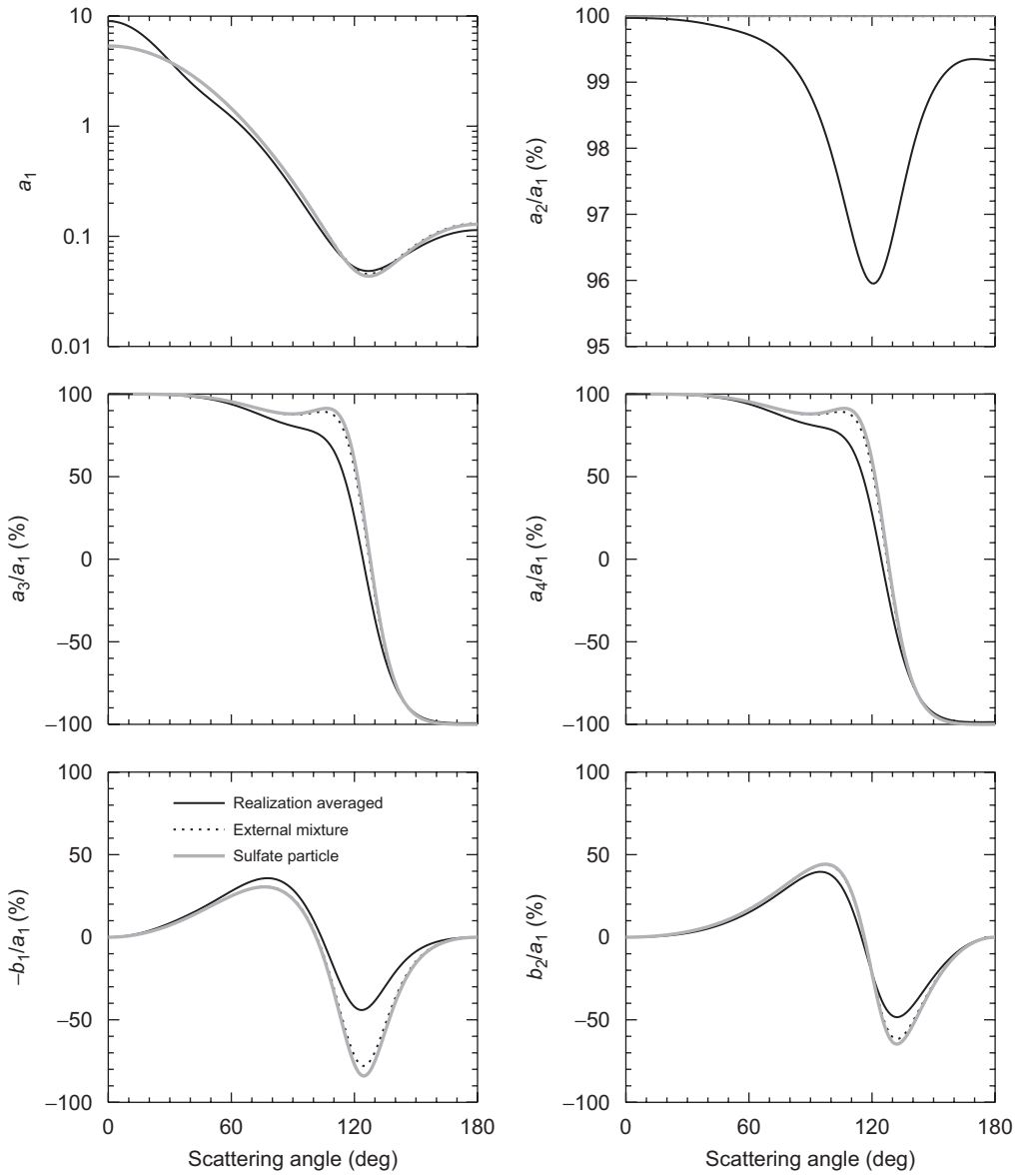

Fig. 5. Ensemble-averaged scattering matrix elements versus scattering angle for aerosols formed by aggregation of soot clusters with a sulfate particle. The soot fractal parameters are $D_f = 2.4$, $k_0 = 1.19$, $N_S = 300$, and $a = 0.02\,\mu m$, and the soot refractive index is $1.75 + i0.435$. The radius and the refractive index of the sulfate particle are $0.2\,\mu m$ and 1.44, respectively. The dotted curves depict the scattering matrix elements for the corresponding external mixture, and the gray curves show the scattering properties of the sulfate particle alone.

geometrical configurations for a variety of composition-equivalent aggregates have a rather weak effect on the integral photometric characteristics.

Fig. 7 illustrates the differences in the scattering matrix elements between the ensemble of 20 aggregate realizations and the corresponding external mixture. The strong oscillations are due to the interference structure typical of monodisperse wavelength-sized spheres [30]. One can see that the relative phase-function differences are rather small. A notable exception is the exact forward-scattering direction, where the constructive interference effects result in a significant enhancement of the aggregate phase function [30]. The strong deviation of the ratio $a_2(\Theta)/a_1(\Theta)$ from 100% and the deviation of the ratios $a_3(180^\circ)/a_1(180^\circ)$ and

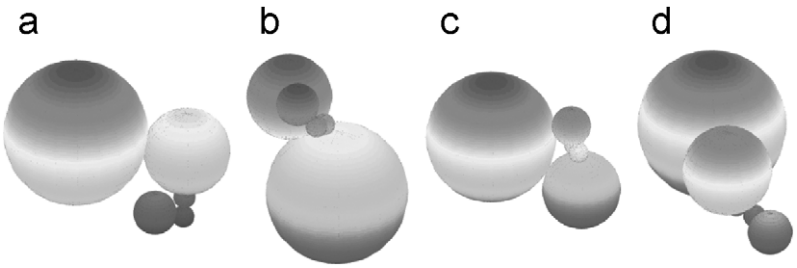

Fig. 6. Multi-component aggregates consisting of two dust particles (refractive index $m = 1.53 + i0.008$, radii $r = 1$ and $0.6\,\mu m$), two equal-sized soot particles ($m = 1.75 + i0.435$, $r = 0.15\,\mu m$), and one sulfate particle ($m = 1.44$, $r = 0.3\,\mu m$).

Table 3
Integral photometric characteristics of multi-component aggregates

Ensemble-averaged value		C_{ext} (μm^2)	C_{abs} (μm^2)	C_{sca} (μm^2)	g	ϖ
		11.2789	1.3624	9.9165	0.7748	0.8792
Ratio		Extinction	Absorption	Scattering	AP[a]	SSA[b]
	Std/mean (%)[c]	0.9705	3.4615	0.7837	0.3886	0.3794
	Ext/aggregate[d]	1.1418	1.1149	1.1455	0.9846	1.0032

[a]Asymmetry parameter.
[b]Single-scattering albedo.
[c]The ratio of one standard deviation to the corresponding value averaged over 20 realizations of the multi-component aggregate.
[d]The ratios of the optical properties calculated for the external mixture to the corresponding aggregate ensemble-averaged values.

$a_4(180^\circ)/a_1(180^\circ)$ from -100% demonstrate once again the inadequacy of using the Lorenz–Mie theory to simulate light scattering by aggregated aerosols.

6. Discussion and conclusions

Our analysis of numerically exact T-matrix results demonstrates that the electromagnetic scattering and absorption characteristics of a single soot-cluster realization represent adequately the properties of the entire ensemble of fractal-parameter-equivalent soot clusters. This implies that the conclusions drawn in [18] apply equally to ensembles of soot clusters. The errors caused by employing the external-mixing approximation and the model wherein a large homogeneous sphere is used to represent a cluster of the same total volume are quite significant, both in the integral photometric characteristics and in the Stokes scattering matrix elements. This suggests that the complex morphology of dry soot aerosols must be explicitly taken into account in remote sensing and radiation balance applications.

Once a soot cluster is attached to a larger nonabsorbing or weakly absorbing particle (e.g., a sulfate, silica, or dust particle), the contribution of soot to the total scattered signal may become relatively small, and the larger particle may dominate light scattering and absorption by the entire aggregate. Aggregation results in larger extinction, absorption, and scattering cross-sections relative to the corresponding external mixture, but by no more than $\sim 20\%$. However, the differences in the scattering-matrix elements can be quite significant, thereby providing an argument against using the external-mixture approximation in remote-sensing applications.

The T-matrix results for aggregates consisting of several components with different sizes and refractive indices are largely consistent with our previous findings for two-particle aggregates [17]. Possibly due to mutual shadowing, the multi-component aggregates are somewhat less effective in scattering and absorbing light than their composition-equivalent external-mixture counterparts. Taking into account relatively small errors in the single-scattering albedo and asymmetry parameter, it appears rather safe to use the external-mixture approximation in radiation balance computations.

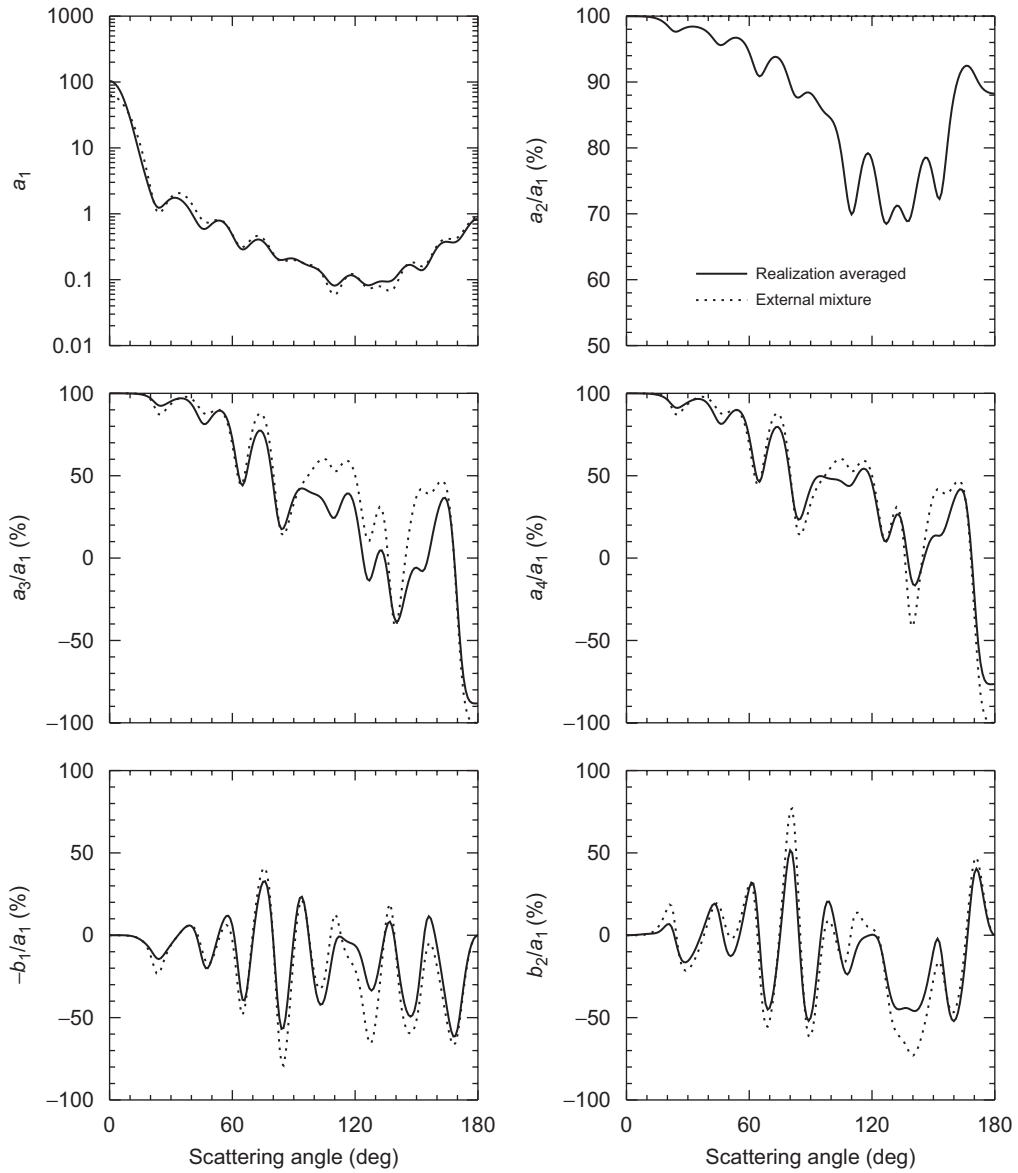

Fig. 7. Ensemble-averaged scattering matrix elements versus scattering angle for 20 composition-equivalent multi-component aggregates consisting of two dust particles, two soot particles, and one sulfate particle (black curves). The dotted curves show the results for the corresponding external mixture.

Acknowledgments

We thank Dan Mackowski for providing the code for generating fractal clusters consisting of hard spheres. This research was funded by the NASA Radiation Sciences Program managed by Hal Maring and by the NASA Glory Mission Project.

References

[1] Nakajima T, Tanaka M, Yamano M, et al. Aerosol optical characteristics in the yellow sand events observed in May, 1982 at Nagasaki. II. Models. J Meteorol Soc Japan 1989;67:279–91.

[2] Li J, Anderson JR, Buseck PR. TEM study of aerosol particles from clean and polluted marine boundary layers over the North Atlantic. J Geophys Res 2003;108:4189.
[3] Li J, Pósfai M, Hobbs PV, Buseck PR. Individual aerosol particles from biomass burning in southern Africa: 2. Compositions and aging of inorganic particles. J Geophys Res 2003;108:8484.
[4] Reid JS, Jonsson HH, Maring HB, et al. Comparison of size and morphological measurements of coarse mode dust particles from Africa. J Geophys Res 2003;108:8593.
[5] Reid EA, Reid JS, Meier MM, et al. Characterization of African dust transported to Puerto Rico by individual particle and size segregated bulk analysis. J Geophys Res 2003;108:8591.
[6] Pósfai M, Gelencsér A, Simonics R, et al. Atmospheric tar balls: particles from biomass and biofuel burning. J Geophys Res 2004;109:D06213.
[7] Clarke AD, Shinozuka Y, Kapustin VN, et al. Size distributions and mixtures of dust and black carbon aerosol in Asian outflow: physiochemistry and optical properties. J Geophys Res 2004;109:D15S09.
[8] Chýlek P, Videen G, Ngo D, Pinnick RG, Klett JD. Effect of black carbon on the optical properties and climate forcing of sulfate aerosols. J Geophys Res 1995;100:16325–32.
[9] Fuller KA. Scattering and absorption cross sections of compounded spheres II. Calculations for external aggregation. J Opt Soc Am A 1995;12:881–92.
[10] Mishchenko MI, Lacis AA, Carlson BE, Travis LD. Nonsphericity of dustlike tropospheric aerosols: implications for aerosol remote sensing and climate modeling. Geophys Res Lett 1995;22:1077–80.
[11] Mishchenko MI, Travis LD, Kahn RA, West RA. Modeling phase functions for dust-like tropospheric aerosols using a shape mixture of randomly oriented polydisperse spheroids. J Geophys Res 1997;102:16831–47.
[12] Fuller KA, Malm WC, Kreidenweis SM. Effects of mixing on extinction by carbonaceous particles. J Geophys Res 1999;104:15941–54.
[13] Mackowski DW. A simplified model to predict the effects of aggregation on the absorption properties of soot particles. JQSRT 2006;100:237–49.
[14] Dubovik O, Sinyuk A, Lapyonok T, et al. Application of spheroid models to account for aerosol particle nonsphericity in remote sensing of desert dust. J Geophys Res 2006;111:D11208.
[15] Mackowski DW, Mishchenko MI. Calculation of the T matrix and the scattering matrix for ensembles of spheres. J Opt Soc Am A 1996;13:2266–78.
[16] Mishchenko MI, Travis LD, Lacis AA. Scattering, absorption, and emission of light by small particles. Cambridge: Cambridge University Press; 2002. (Available on-line at http://www.giss.nasa.gov/~crmim/books.html.)
[17] Mishchenko MI, Liu L, Travis LD, Lacis AA. Scattering and radiative properties of semi-external versus external mixtures of different aerosol types. JQSRT 2004;88:139–47.
[18] Liu L, Mishchenko MI. Effects of aggregation on scattering and radiative properties of soot aerosols. J Geophys Res 2005;110:D11211.
[19] Sorensen CM. Light scattering by fractal aggregates: a review. Aerosol Sci Technol 2001;35:648–87.
[20] Kolokolova L, Kimura H, Ziegler K, Mann I. Light-scattering properties of random-oriented aggregates: do they represent the properties of an ensemble of aggregates? JQSRT 2006;100:199–206.
[21] Mishchenko MI, Videen G, Babenko VA, et al. T-matrix theory of electromagnetic scattering by particles and its applications: a comprehensive reference database. JQSRT 2004;88:357–406.
[22] van de Hulst HC. Light scattering by small particles. New York: Wiley; 1957.
[23] Mikhailov EF, Vlasenko SS, Kiselev AA. Optics and structure of carbonaceous soot aggregates. In: Markel VA, George TF, editors. Optics of nanostructured materials. Hoboken, NJ: Wiley; 2001. p. 413–66.
[24] Sorensen CM, Roberts GC. The prefactor of fractal aggregates. J Colloid Interface Sci 1997;186:447–52.
[25] Charalampopoulos TT. Morphology and dynamics of agglomerated particulates in combustion systems using light scattering techniques. Prog Energy Combust Sci 1992;18:13–45.
[26] d'Almeida GA, Koepke P, Shettle EP. Atmospheric aerosols: global climatology and radiative characteristics. Hampton, VA: Deepak; 1991.
[27] Klusek C, Manickavasagam S, Mengüç MP. Compendium of scattering matrix element profiles for soot agglomerates. JQSRT 2003;79/80:839−59.
[28] West RA. Optical properties of aggregate particles whose outer diameter is comparable to the wavelength. Appl Opt 1991;30:5316–24.
[29] Ebert M, Weinbruch S, Rausch A, et al. Complex refractive index of aerosols during LACE 98 as derived from the analysis of individual particles. J Geophys Res 2002;107:8121.
[30] Mishchenko MI, Mackowski DW, Travis LD. Scattering of light by bispheres with touching and separated components. Appl Opt 1995;34:4589–99.